



Microstructure-Hardness Relationships in Subzero Quenched and Aged TC21 α/β Titanium Alloy



Rania M. El-Shorbagy^{1*}, Abdel Hamid A. Hussein¹, E. M. El-Banna¹,
Z. M. El-Baradie², and M. A. Waly²

¹Department of Mining, Petroleum and Metallurgical Engineering, Faculty of Engineering, Cairo University, Giza 12613, Egypt.

²Central Metallurgical Research and Development Institute, Helwan, Egypt.

TITANIUM alloys have long been recognized as outstanding strong, light and corrosion resistant alloys. TC21 alloy has recently received considerable attention due to its high strength, toughness, damage-tolerance properties and low crack propagation rate. Similar to steels, titanium alloys have demonstrated their capacity to produce martensitic microstructure upon suitable heat treatment. Their martensite and its transformations upon subsequent heat treatment proved to be an important tool to obtain controllable properties. The martensite (start) characteristic temperature (M_s) has received some attention as regards its dependence on composition. On the other hand, no similar attention was given to the dependence of the other important martensitic (finish) characteristic temperature (M_f) on composition. In view of the foregoing, this work was thus planned to fulfill this lacking information via subzero hardening treatments of TC21 α/β alloy. Detailed analysis of the so obtained microstructures via optical and scanning microscopy, and x-ray diffraction data has led to a quantitative estimation of the M_f temperature and its composition dependence. Additionally, the hardening effect of those subzero hardening treatments was studied via hardness and microhardness measurements. Significant findings were recorded which are expected to help reaching useful property levels such as strength, wear resistance and damage-tolerance.

Keywords: TC21 α/β titanium alloy, Subzero hardening, Microstructure, Titanium martensite, Phase transformation, Aging, Hardness, Microhardness.

Introduction

Over the past decades, titanium alloys are considered high-quality structural materials [1-4]. They are used in the airframe and aircraft engines due to their excellent mechanical properties, relatively low density and creep resistance [4-15]. Moreover they are ideal materials for biomedical, marine, petroleum, chemical, pharmaceutical and other industries due to good corrosion resistance [11, 16]. In the aerospace field, the design criteria of structural components have changed from static strength design to damage-tolerance design in order to satisfy the performance requirement of the high-quality structural materials such as high strength, fracture toughness and low crack growth rate [2, 14-15]. As a new titanium alloy, TC21 alloy is a new category of α/β titanium alloys with high strength, toughness, and damage-

tolerance properties, and usually considered to be more difficult to process due to higher yield/tensile ratio and lower elastic modulus [13-14, 17-23]. Recently, TC21 alloy has been successfully developed as a structural material in aerospace applications mainly located in the landing gear system as well as in connections between wing and fuselage [24]. In case of using TC21 alloy as important structural aircraft parts such as landing gear and flap track, there will be a significant advantage on weight loss for the aircraft [23, 24]. This alloy was reported to have strength of 1050-1200 MPa and fracture toughness of ~ 72 MPa. $m^{1/2}$ [18]. The mechanical properties of TC21 alloys normally rely on their microstructures, characteristics such as grain size, phase fraction, phase morphology and phase distribution, etc. [19, 25]. Upon cooling from the high temperature β phase in such alloys, some phase changes occur

*Corresponding author e-mail: eng.raniamohamed10@gmail.com

Received 16/10/2019; Accepted 5/11/2019

DOI: 10.21608/ejchem.2019.18279.2125

©2020 National Information and Documentation Center (NIDOC)

depending on the cooling rate. Fast cooling rate tends to produce martensite whereas moderate rates tend to affect the morphology of the β/α transformation [26]. The transformation of β phase to martensite begins when the martensite start temperature (M_s) is reached resulting in a homogeneous transformation of the β phase into the hexagonal α' martensite. Increasing the solute content the α' structure of the martensite become distorted and the structure described as orthorhombic α'' . The type and amount of α' or α'' that forms with quenching is dependent on the chemistry of the β phase prior to quenching. Those alloys with increasing β stabilizing elements have a higher tendency to form α'' instead of α' [27]. Some authors reported that orthorhombic α'' martensite was formed in TC21 alloy after solution treatment above 840 °C [23].

In contrast to the measurable hardening caused by martensite in steels, only moderate hardening takes place by martensite in titanium alloys [28]. It is therefore worthwhile to investigate proper heat treatments namely leading to martensitic transformation and their impact on alloy hardening. Relevant hardness measurements would therefore be of particular value especially when one considers the correlation of hardness and strength. Unfortunately, researches on the mechanical properties of Ti alloys containing martensite and its consequent microstructural evolution via heat treatment conditions is rather limited. Accordingly, this work attempts to contribute to this lack of information in TC21 titanium alloy via studying the influence of subzero heat treatments on martensite formation and its accompanying microstructural changes. The heat treatment cycles will be tailored to study the interrelations of high quench temperatures, subzero temperatures, aging treatments and their role in microstructural development and effect on properties.

Experimental work

Material:

The TC21 titanium alloy used in this study was received from Baoji Hanz Material Technology Co. Ltd., China* as bars of 7 mm diameter and 140 mm length. The chemical composition (wt. %) of the as-received alloy is listed in Table 1. The measured β transus temperature (T_β) of this alloy is close to 955°C [29]. Disc-shaped specimens with 5 mm in height were cut using wire electrical

discharge machine (EDM). Such specimens were used for the heat treatment conditions as well as microstructural examinations.

Heat treatment:

In order to perform efficient heat treatment cycles, the heat treatments were performed using a vertical tube furnace where the specimens were allowed to fall directly into the quenching medium with a minimum of delay time. Additionally, a calibrated K type thermocouple was inserted into the middle of the furnace where the sample was placed during all heating conditions to ensure that the samples require the correct preset temperature. The specimens were heated at preset annealing temperatures, (900°C, 940°C and 980 °C), held for 20 min followed by quenching to media adjusted at the following temperatures: a) water at room temperature (25 °C), b) Icy water (0 °C), c) Dry ice/alcohol adjusted at -20 °C and d) Dry ice/alcohol adjusted at -40 °C. A post aging treatment was applied at 520 °C for 5 hr in all specimens. The aging treatment was performed in a salt bath to ensure a homogeneous temperature distribution around the specimens. Schematic drawing of the experimental procedure for the heat treatment cycle is shown in Figure 1.

Microstructure examination:

A detailed metallographic examination was performed utilizing both OLYMPUS BX41M-LED optical microscope (OM) and QUANTA FEG 250 scanning electron microscope (SEM). The samples for metallographic examination were prepared by mechanical polishing and then etching using Kroll's reagent containing 10 mL HF, 5 mL HNO₃ and 85 mL water. X-ray diffraction (XRD) analysis was conducted on finely polished samples to identify the present phases using ARL X'TRA x-ray diffractometer with Cu K α radiation. The volume fraction of α phase was estimated by using image analyzer software. Lineal analysis was adopted for grain size determination. Vickers hardness measurements were carried out using Vickers hardness tester (ZWICK/ROELL ZHU 250) in accordance to ASTM E384-11 standard, under a load of 10 kg for 15 s. Additionally, microhardness measurements were performed using Vickers microhardness tester, with a load of 100 gm for 10 s. For all hardness values an average of five readings was determined. Such average values are good within ± 5 .

Results and Discussion

Microstructure analysis:

As-received material:

The microstructure of the as-received TC21 sample is shown in Figure 2. The dark regions appearing in SEM micrograph correspond to the primary α phase, in both equiaxed and acicular form, whereas the bright regions are β -phase. A homogeneous distribution of both phases can be noticed. These microstructure constituents have been previously reported by several authors [5, 25, 29-31]. It is found that the average grain size of α phase was in the range of 2-2.5 μm and its volume fraction approached 65%.

The corresponding x-ray diffraction pattern of the as-received alloy is shown in Figure 3. The XRD pattern confirmed the presence of a majority of α and less dominant β phase, apparently no other phases are present which confirm the levels of volume fractions of both phases as detected metallographically. These results are in accord with previous work [25, 30].

Samples quenched from 940 °C to subzero temperatures:

After quenching from 940 °C to 0 °C, the microstructure consists of a combination of α grains having the as received morphology plus widmanstatten α grains as appears in Figure 4a. Decreasing the quench medium temperature to -20 °C, the widmanstatten morphology of α phase appears to be overwhelming, Figure 4b. On the other hand, after quenching from 940 °C to -40 °C, the as quenched microstructure appears to be largely martensitic, Figure 4c. The prior β grain boundaries are resolved and a grain size of $\sim 315 \mu\text{m}$ is recorded. This finding confirms that the β phase composition at 940 °C has M_f temperature close to -40 °C. This conclusion is further confirmed by the XRD data of Figure 5, where the chart exhibits mostly α'' martensite peaks. The volume fraction of the α phase at 940 °C was estimated at 26% measured by quenching to room temperature.

Samples quenched from 980 °C to subzero temperatures:

After raising the quench temperature to 980°C (25 °C above the β -transus), and quenching to 0 °C, the microstructure (Figure 6a) is largely

martensitic with little retained β phase as also detected by XRD, Figure 7. The weak intensity of the β peaks reflects the presence of a little amount of retained β phase. This finding refers to M_f temperature below 0 °C. The retained β phase may be entrapped between the martensite plates. It was reported that the diffusionless $\beta \rightarrow \alpha'$ transformation occurred during cooling at 23.1°C/s (corresponding to quenching in icy water) from 1020°C for Ti6Al4V alloy although the complete transformation of β into α' had been reported to take place in the Ti6Al3Mo, Ti6Al3Mo1V and Ti6Al2Mo2Cr alloys after cooling at 40°C/s [8]. By lowering the subzero temperature to -20 °C (Figure 6b), the microstructure appears to be fully martensitic. The XRD pattern shows mostly peaks of α'' martensite. This means that -20 °C is close to the M_f temperature of the present TC21 alloy. Further lowering of the quench medium temperature to -40 °C (Figures 6c and d) leads to the formation of fully martensitic structure as evidenced by the XRD pattern. In all the three cases mentioned, the prior β grain size ranges from 311 to 348 μm .

Estimation of M_f martensite characteristic temperature:

Based on the forgoing experimental findings, namely the detection of martensite after subzero quenching, it is worthwhile to estimate the M_f martensite temperature as a function of alloy composition, particularly as no relevant information was reported in previous work. Figure 8 demonstrates the M_f values as determined for the two cases quenched from 980 and 940 °C as a function of the molybdenum equivalent $[\text{Mo}]_{\text{eq}}$ [32]. This parameter is based on the strong β stabilizing effects of Mo, Cr and Nb. Points 1 and 2 represent two determined values and point 3 is determined by extrapolation of the line joining 1 and 2 and the value of $[\text{Mo}]_{\text{eq}}$ is determined from the composition of corresponding β phase. Based on this linear ($M_f - [\text{Mo}]_{\text{eq}}$) relationship, the following equation may be assumed:

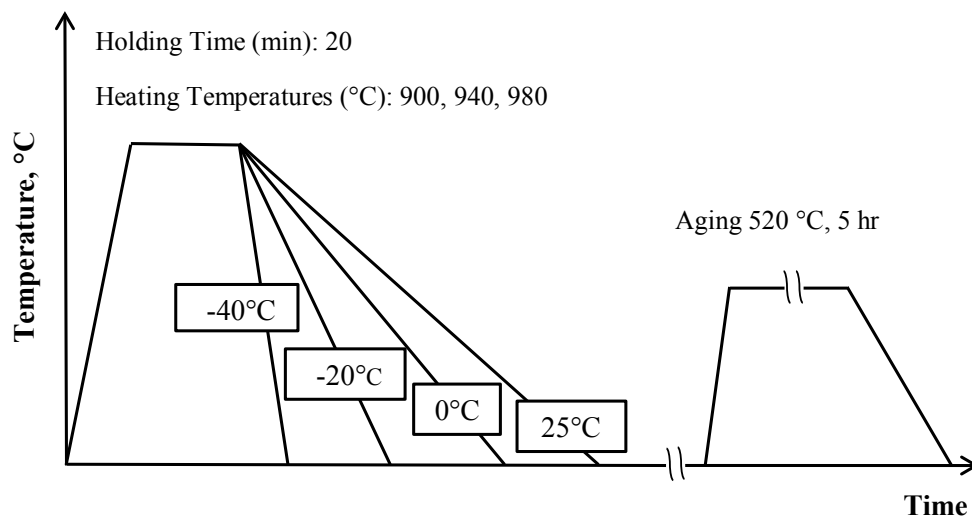
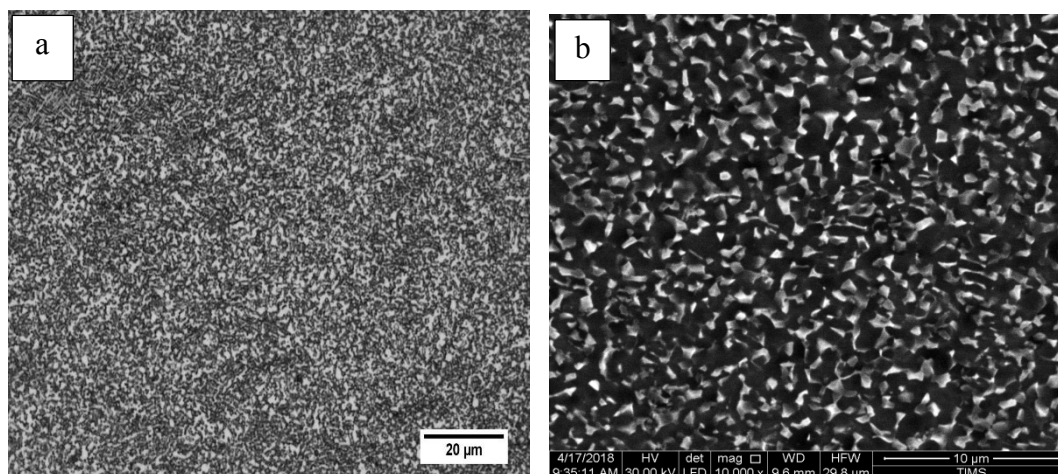
$$M_f (\text{°C}) = -19.80 [\text{Mo}]_{\text{eq}} + 86.93$$

Aging condition:

In most cases, the aging treatment is done to improve the ductility of the alloy after solution treatment and quenching [33]. Solution treatment and quenched TC21 alloys are mostly high strength alloys since they contain α'' martensite

TABLE 1. Chemical composition of as-received TC21 Ti-alloy (wt. %)

Al	Mo	Nb	Sn	Zr	Cr	Si	Fe	C	N	H	O	Ti
6.5	3.0	1.9	2.2	2.2	1.5	0.09	0.05	0.01	0.01	0.001	0.07	Bal.

**Fig. 1.** Schematic drawing of the experimental heat treatment cycles.**Fig. 2.** Micrographs of the as-received TC21 alloy: (a) Optical and (b) SEM images.

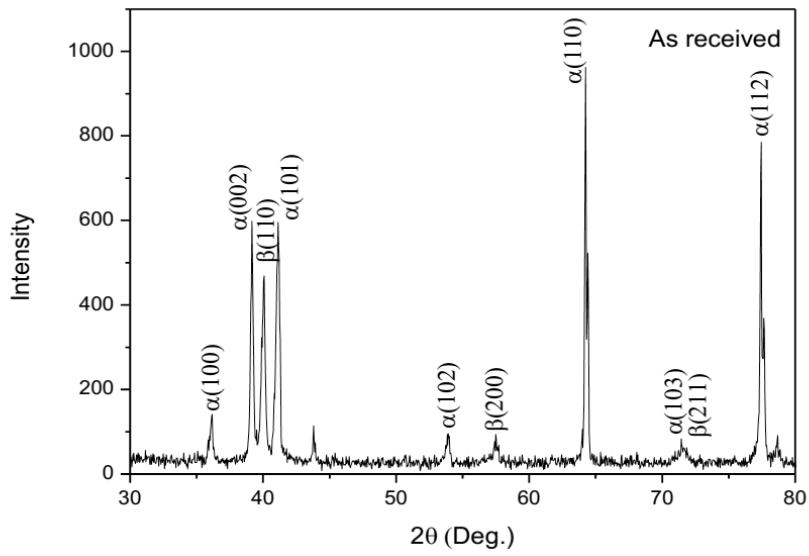


Fig. 3. XRD pattern of the as-received TC21 alloy.

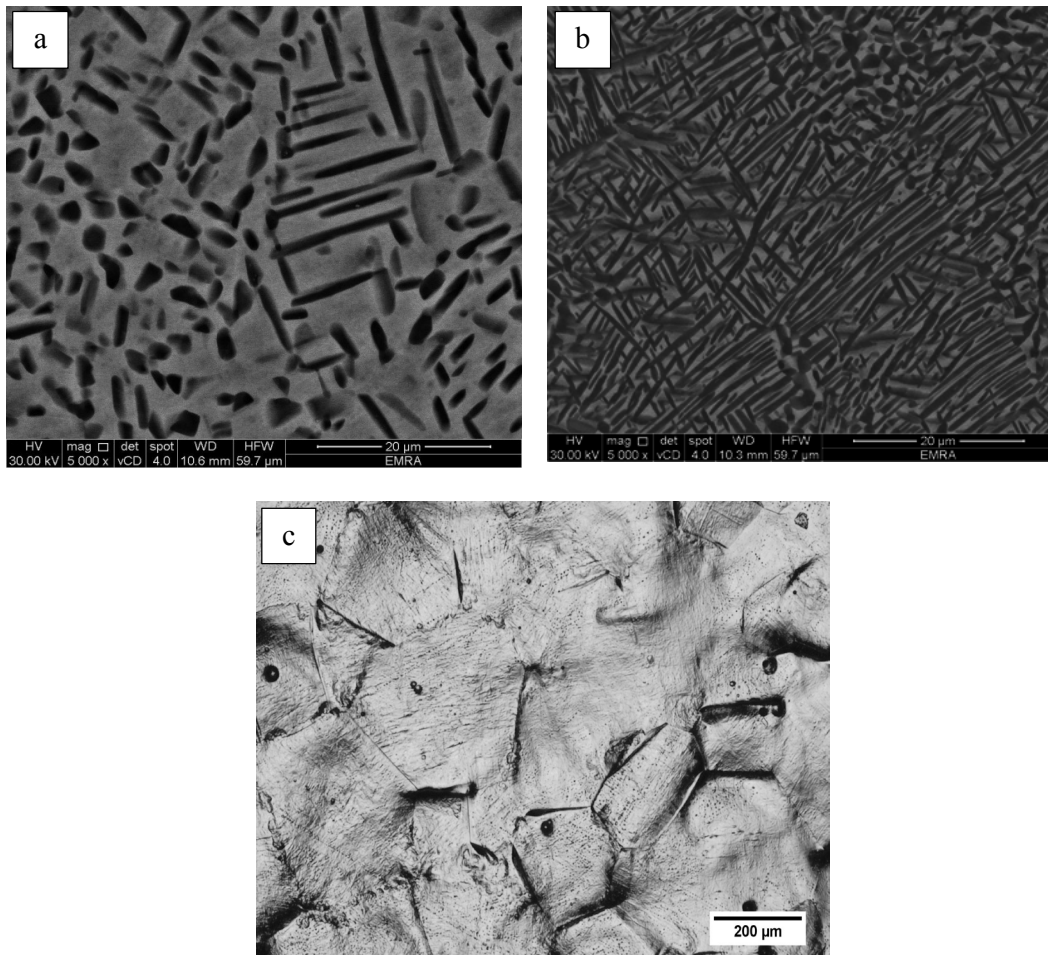


Fig.4. SEM micrographs of samples quenched from 940 °C to: a) 0 °C, b) -20 °C and c) Optical micrograph of the sample quenched from 940 °C to -40 °C.

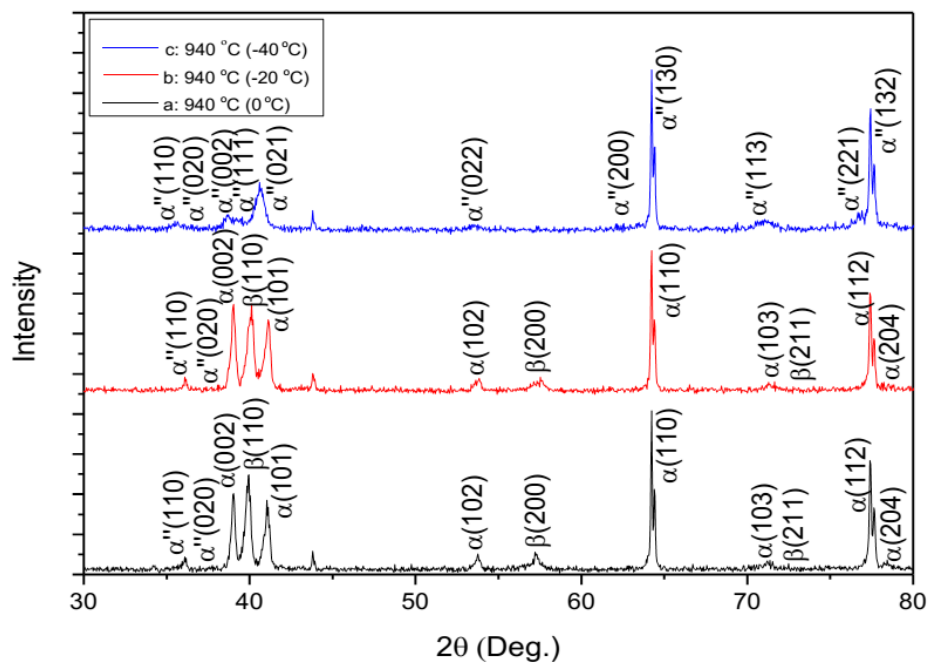


Fig. 5. XRD patterns of samples quenched from 940 °C to subzero temperatures (0, -20 and -40 °C).

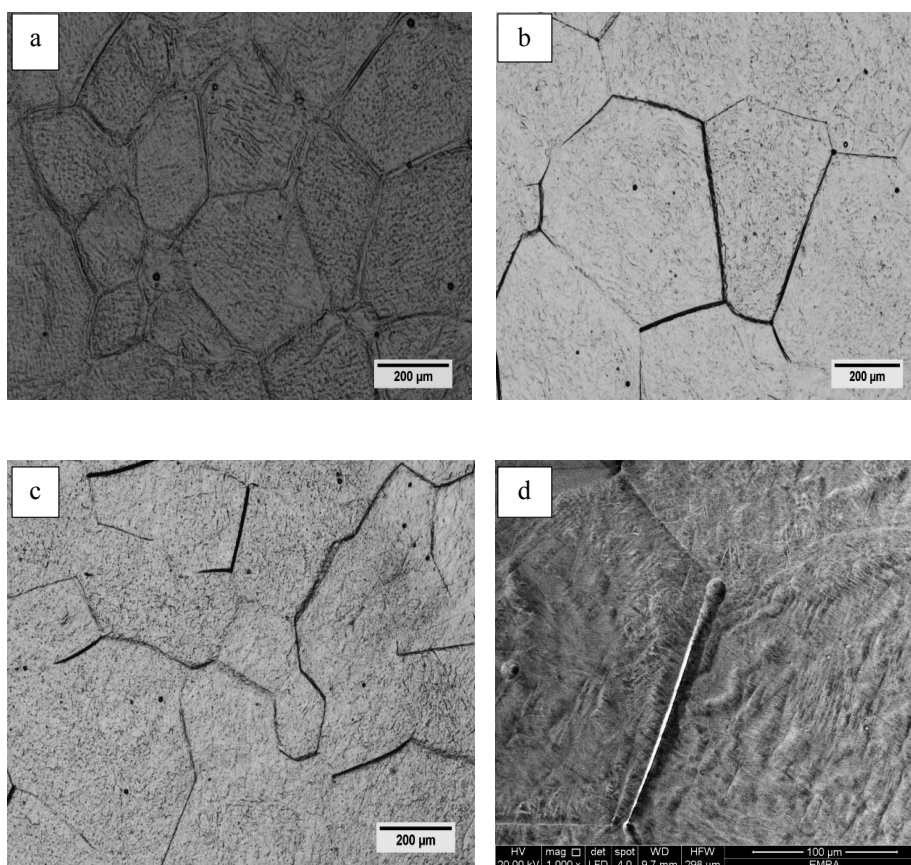


Fig. 6. Optical micrographs of samples quenched from 980 °C to: a) 0 °C, b) -20 °C, c) -40 °C, and d) SEM micrograph of the sample quenched from 980 °C to -40 °C.

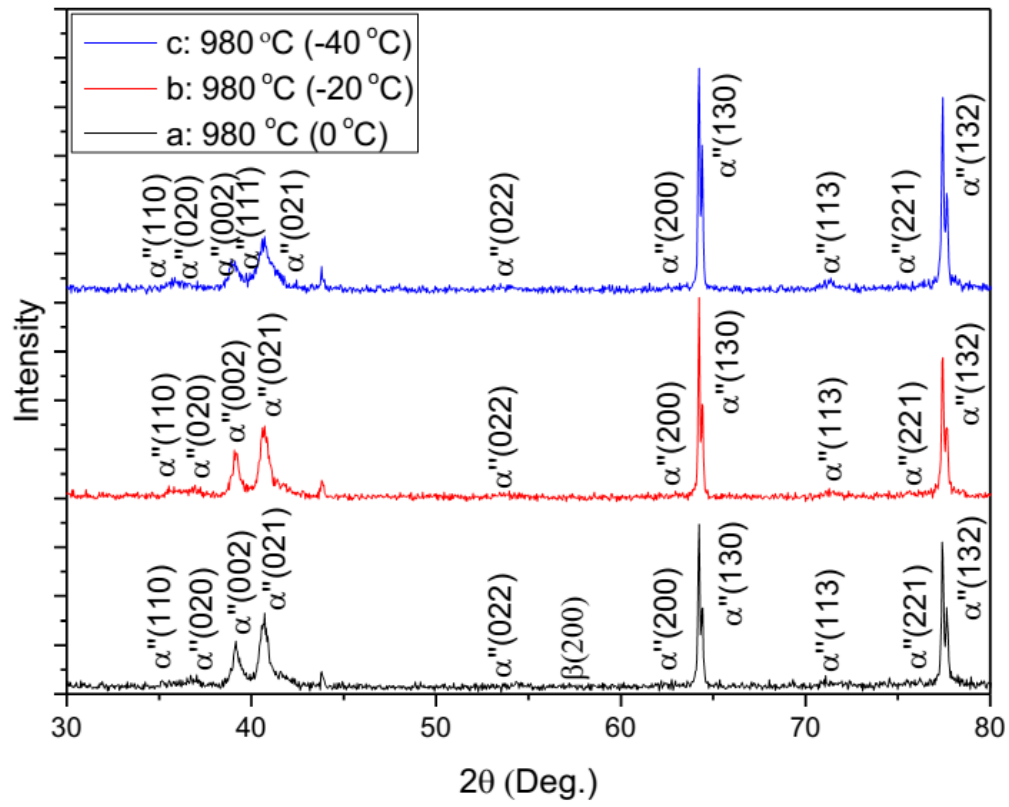


Fig. 7. XRD patterns of samples quenched from 980 °C to subzero temperatures (0, -20 and -40 °C).

which makes the alloy brittle, hence increasing the need for an aging treatment to improve the ductility. Understanding how microstructure changes with the aging treatment, can aid in optimizing the microstructural morphology in TC21 alloys.

Figures 9, 10 and 11 show typical optical and SEM images of aged samples after quenching from 940°C to (0, -20 and -40°C). For the aged sample quenched to 0°C, Figure 9, the secondary α precipitated in the residual β phase and little equiaxed primary α is distributed through the β matrix. Meanwhile, for the aged sample quenched to -20°C, Figure 10, the morphology is largely changed. The residual β matrix becomes clear, and the fine secondary α plates precipitated during aging can be observed in the residual β matrix while the equiaxed α phase disappeared. Similar results obtained for aged sample quenched to -40°C, Figure 11, where fine secondary α phase has precipitated during aging treatment. Also, the equiaxed α phase disappeared. The phases mentioned are also confirmed by XRD patterns shown in Figure 12.

Figures 13, 14 and 15 show the optical and SEM images of aged samples prequenched from 980°C to (0, -20 and -40 °C). Upon aging, the decomposition from the fully martensitic structure into fine secondary α is observed for all samples. Furthermore, the fineness of the α plates become more pronounced as the subzero temperature is lowered from 0 to -40 °C. These results are in agreement with the XRD results shown in Figure 16.

Hardness data:

Quenched samples:

The hardness data obtained in subzero quenched samples from the temperatures 940 °C and 980 °C are compiled in Figure 17. Samples quenched from 940 °C to 0 °C exhibit a relatively low hardness value of HV327. This may be due to the presence of a measurable primary α phase. Upon quenching to -20 °C, the hardness is largely increased to HV397, i.e higher by 21.4% over the previous value at 0 °C. This reflects the large increase of the amount of acicular α'' martensite as the temperature goes down to -20 °C. After quenching to -40 °C, the hardness is practically unchanged (HV399). This finding confirms that -40 °C is nearly close to the martensitic finish temperature (M_f) for the sample quenched from 940 °C.

On the other hand, the quenching from 980 °C to 0 °C exhibits a higher hardness value of HV375, which is due to the increasing amount of martensite as the temperature approaches M_f . Upon decreasing the temperature of quenching medium to -20 °C, the hardness is increased to HV393, i.e. about 5 % increase compared to the hardness value of the sample quenched from 980 °C to 0 °C. This increase in hardness value emerges from the decrease in the amount of retained β phase and the accompanying increase in the amount of acicular α'' martensite. This means that -20 °C is nearly close to the martensite finish temperature (M_f) for the sample quenched from 980 °C.

Meanwhile, the hardness value for sample quenched from 980 °C to -40 °C is slightly decreased about 5.3 % (HV373) compared with the hardness value of the sample quenched from 980 °C to -20 °C. The reason behind this slight decrease in hardness is not yet clear.

Aged condition:

Aging experiments were done on solution treated and water quenched samples due to the consistent hardness values, i.e. the homogeneous structure that had been produced. Water quenching from the solution treatment provides more degrees of freedom in optimizing the microstructure and mechanical properties than air cooling or furnace cooling during aging treatment. It is already determined that quenched microstructures can consist of α , α'' and β phases which would respond better during aging. The presence of fine martensitic needles in solution treated and water quenched samples is desirable for a high ductility, high ultimate tensile strength and consistency in the microstructure as well as providing maximum response during aging [33].

The present aging data are presented as hardness levels in Figure 18. The incremental increase in hardness after aging is well presented in Figure 19. For example, the hardness was increased by 50.5% for the alloy quenched from 940 °C to 0 °C and increased by 32% for the alloy quenched from 940 °C to -20 °C. This is because these alloys contain both secondary α and residual β phases, in addition to the fine-grained $\alpha+\beta$ equilibrium phases produced during aging treatment. On the other hand, the hardness was increased by 31% for the alloy quenched from 940 °C to -40 °C, and by 37% for the alloy quenched from 980 °C to -20 °C and increased by 40.5% for the alloy quenched

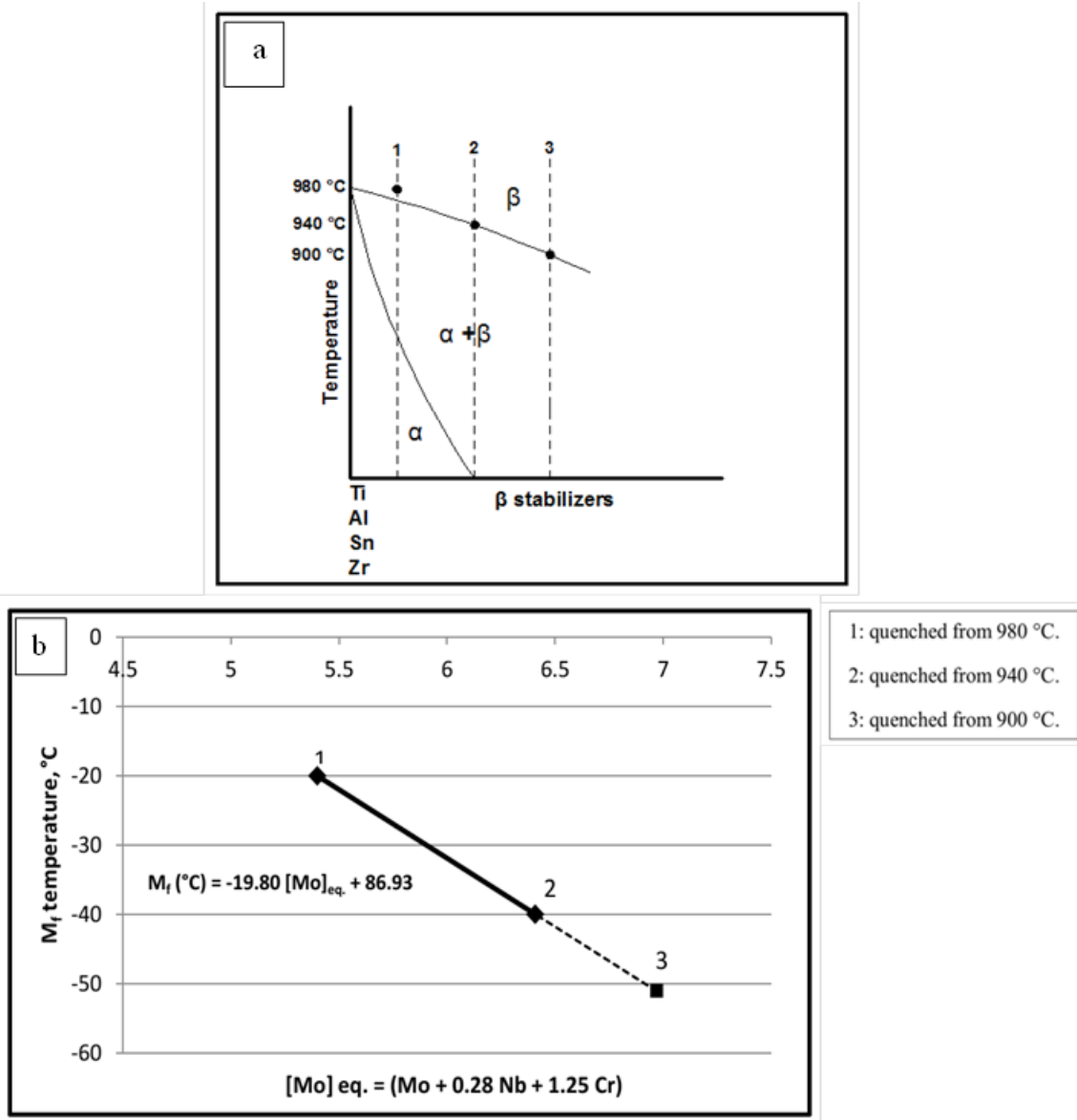


Fig. 8. (a) Hypothetical phase diagram illustrating the location of quench temperatures and composition of the corresponding β phase, and (b) Variation of M_f temperature with $[\text{Mo}]_{\text{eq.}}$ as calculated from the composition of the corresponding β phase at each quench temperature, where :point (1) Based on the original composition (quenched $T_q > T_\beta$), point (2) β composition based on EDX analysis of martensite, and point (3) β composition, extrapolated.

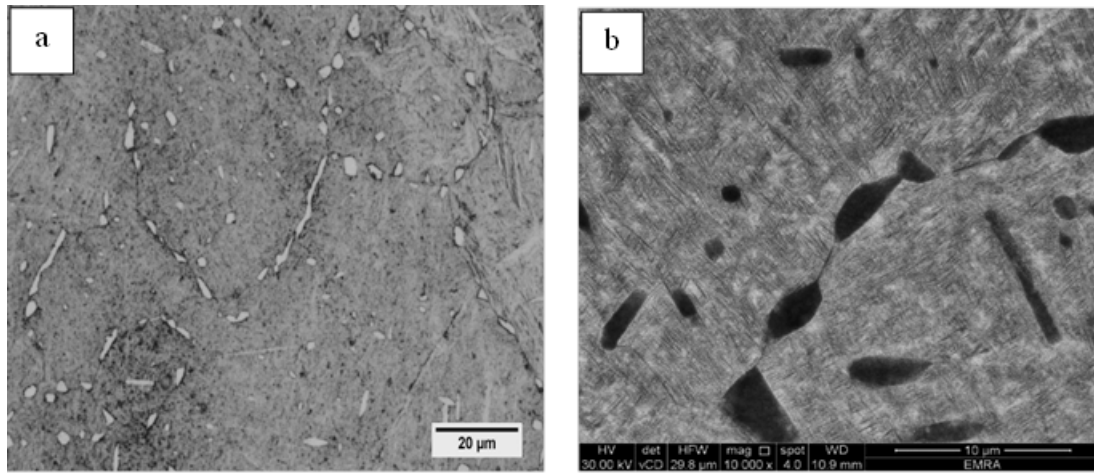


Fig. 9. Micrographs of aged sample prequenched from 940 °C to 0 °C: a) Optical image and b) SEM image.

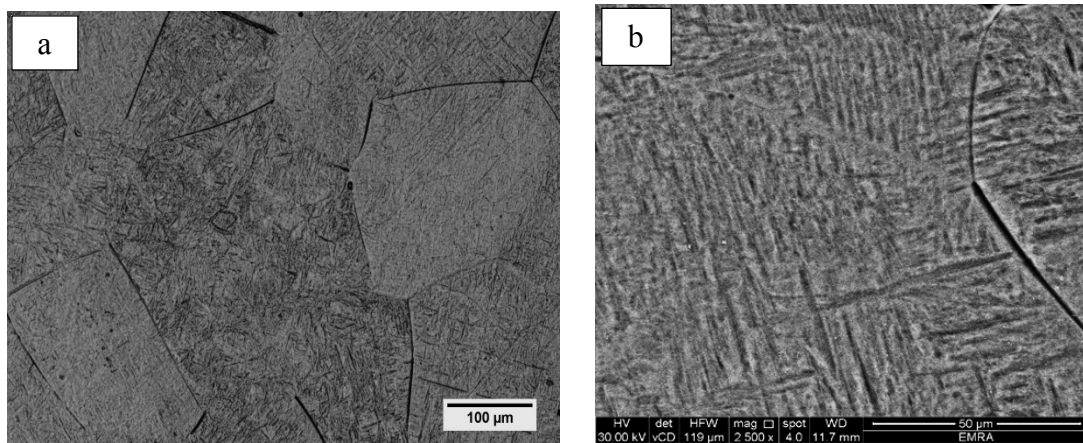


Fig. 10. Micrographs of aged sample prequenched from 940 °C to -20 °C: a) Optical image and b) SEM image.

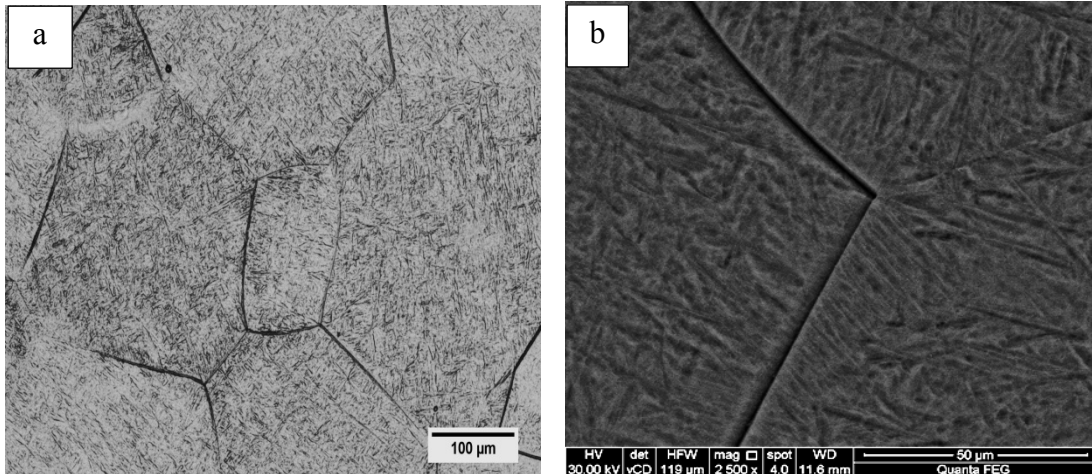


Fig. 11. Micrographs of aged sample quenched from 940 °C to -40 °C: a) Optical image and b) SEM image.

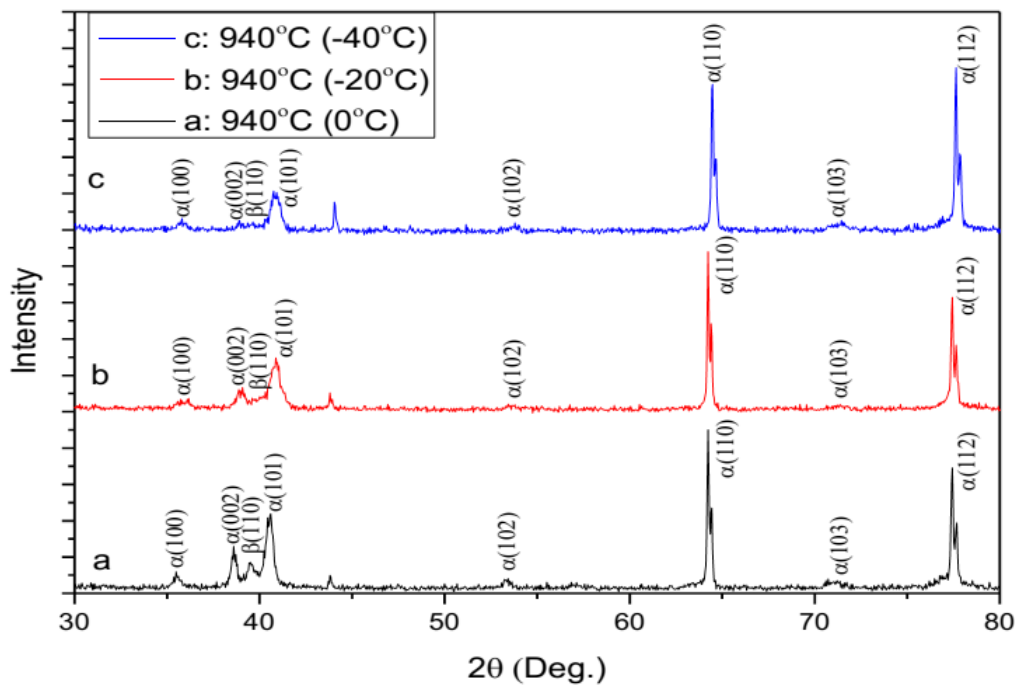


Fig. 12. XRD patterns of the aged samples quenched from 940 °C to subzero temperatures (0, -20 and -40 °C).

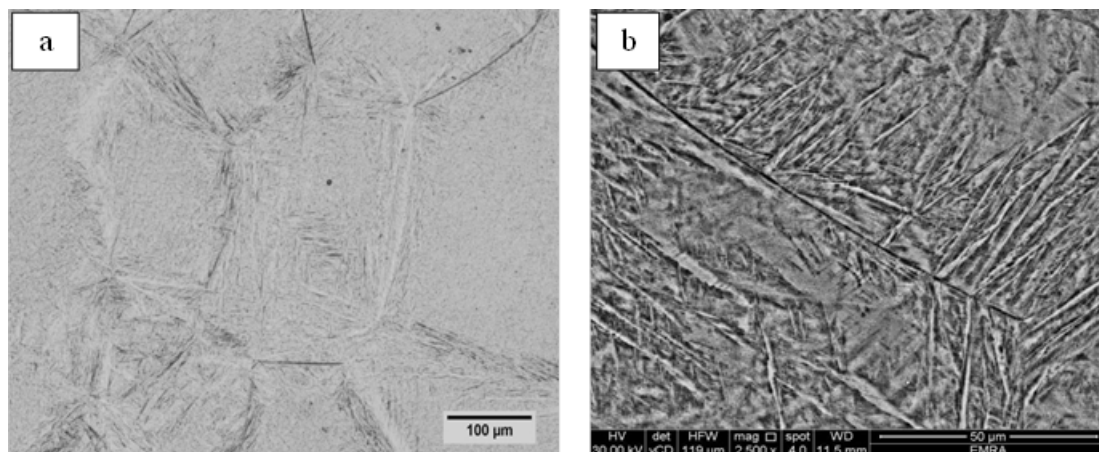


Fig. 13. Micrographs of aged sample prequenched from 980 °C to 0 °C: a) Optical image and b) SEM image.

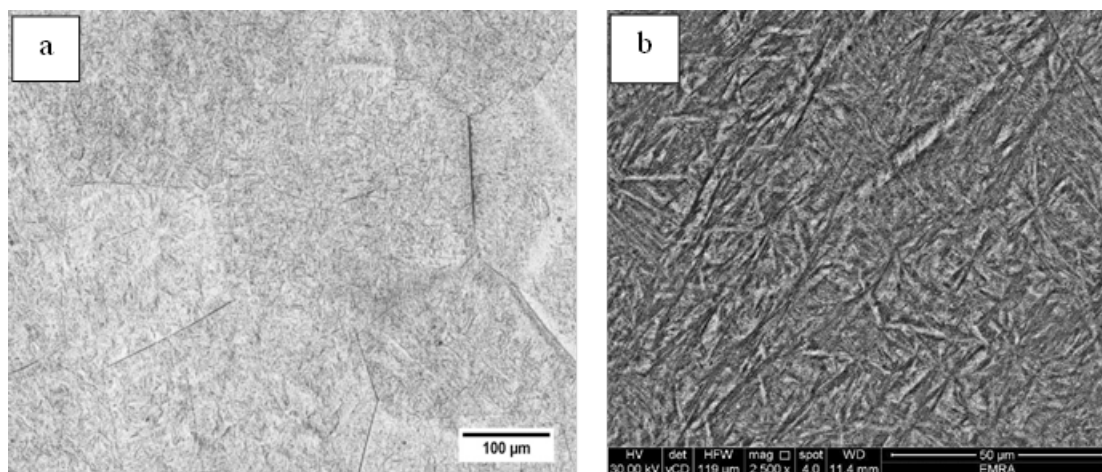


Fig. 14. Micrographs of aged sample prequenched from 980 °C to -20 °C: a) Optical image and b) SEM image.

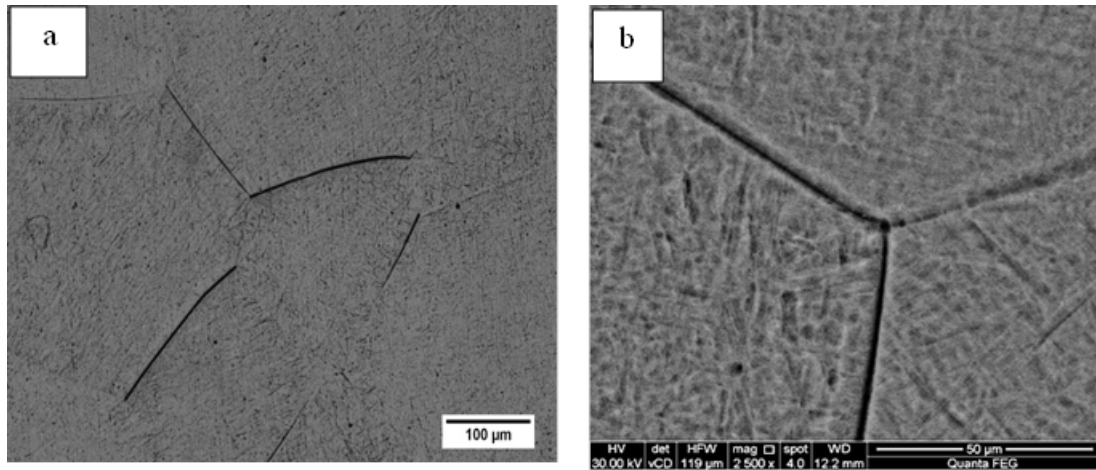


Fig. 15. Micrographs of aged sample prequenched from 980 °C to -40 °C: a) Optical image and b) SEM image.

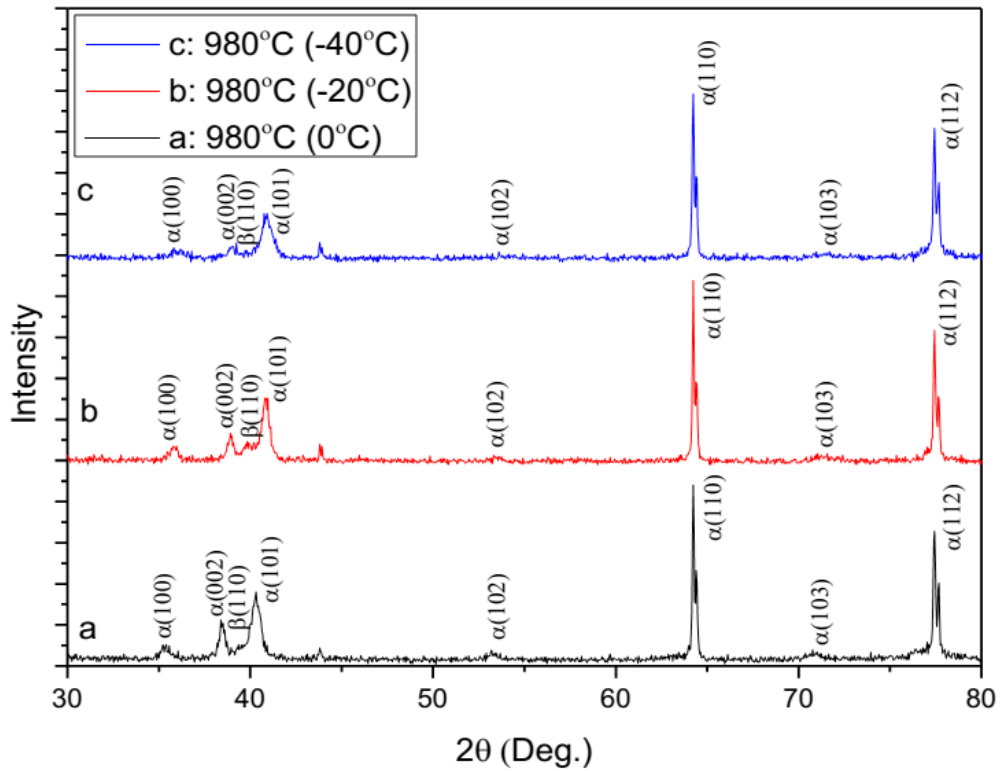


Fig. 16. XRD patterns of the aged samples prequenched from 980 °C to the subzero temperatures (0, -20 and -40 °C).

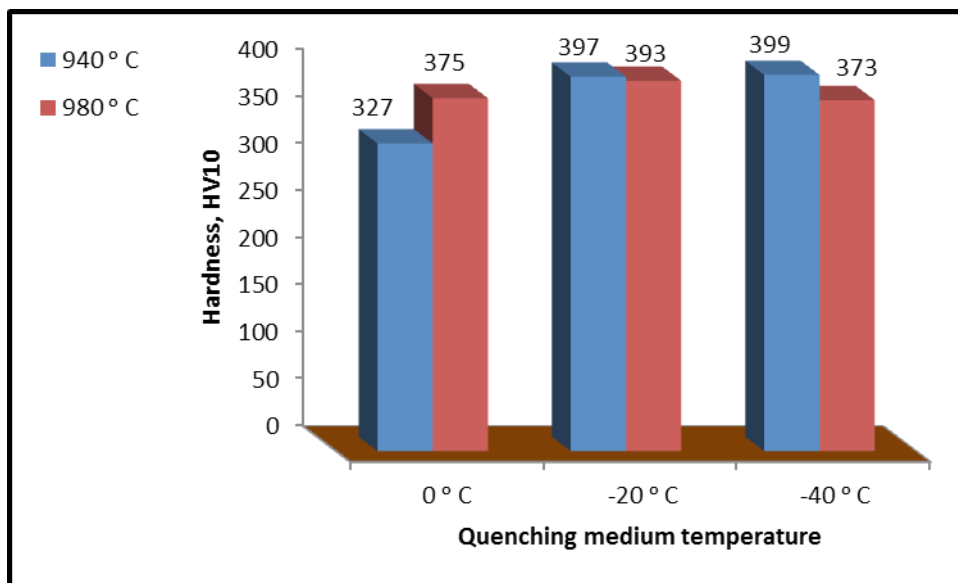


Fig. 17. Average hardness values of as-quenched samples.

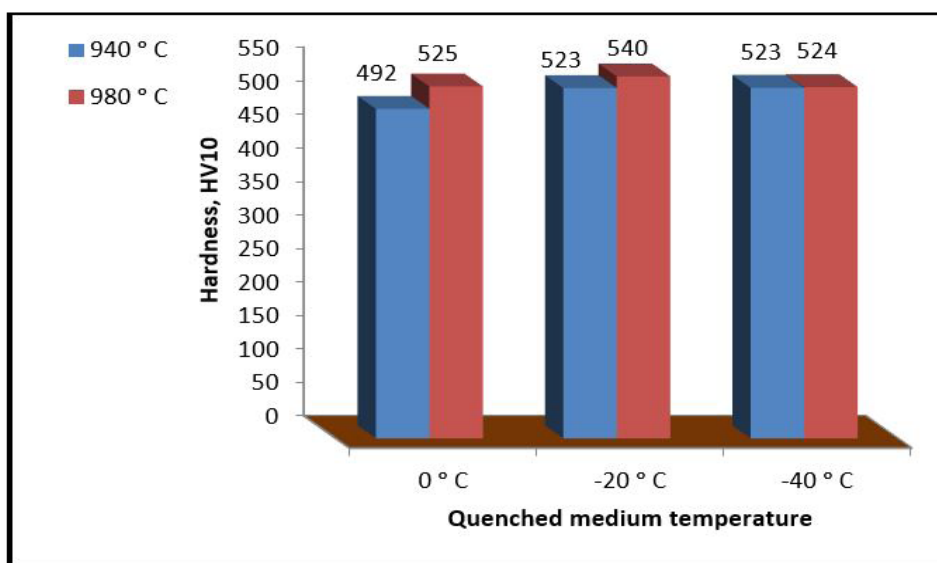


Fig. 18. Average hardness values of aged samples.

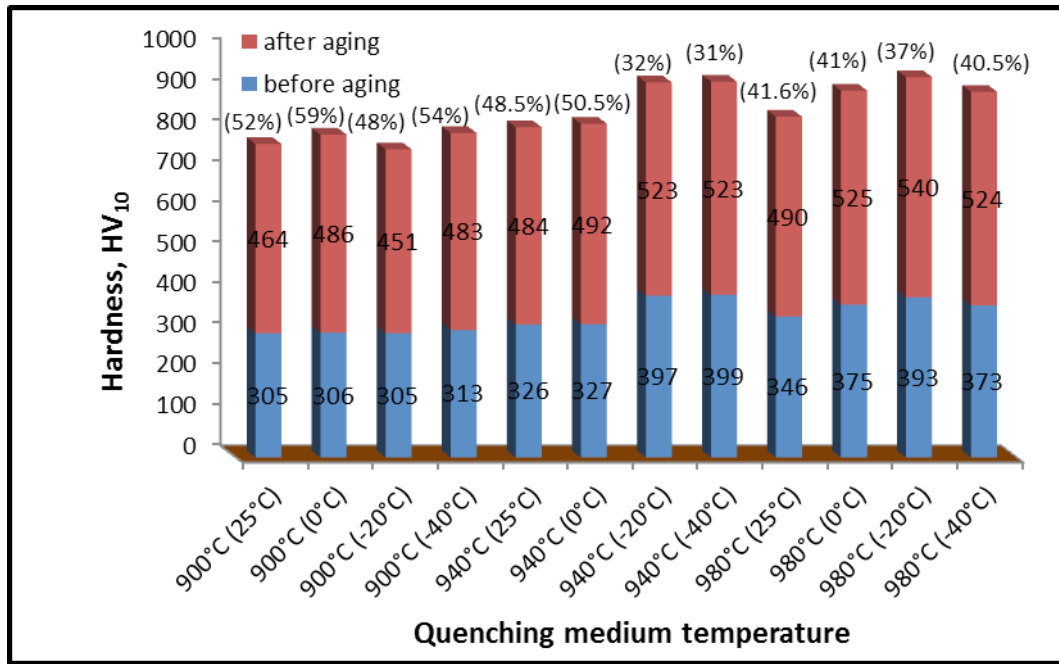


Fig. 19. Comparison of hardness values before and after aging.

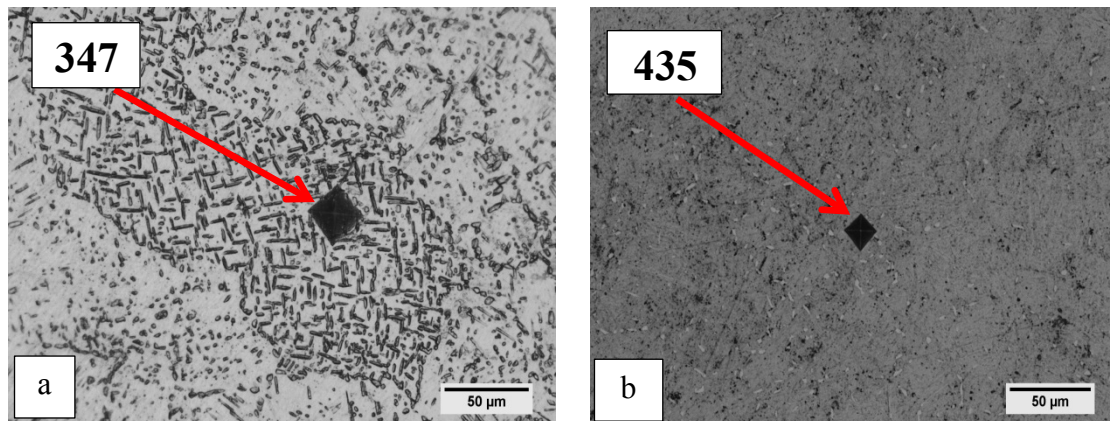


Fig. 20. Photomicrographs of microhardness indentations of: a) Sample quenched from 940 °C to 0 °C, and b) Aged condition.

from 980 °C to -40 °C. Again, such alloys contain measurable amounts of both secondary α and residual β phases produced during aging and due to the fineness of the secondary α with lowering the subzero temperature.

Thus, the general trend is that the hardness is increased due to aging by values from 31 to 50% which is consistent with the microstructure results. During aging treatments, an adjustment of the β and α phases takes place via the partitioning of α and β stabilizing elements between α and β phases. As a result, secondary α platelets form which create extra interphase boundaries. Such boundaries act as barriers to dislocation motion which naturally cause strengthening of the alloy. An increase of residual β matrix which is strengthened by the secondary α platelets tend to increase the α/β phase boundaries and obviously the strength of TC21 alloy also increased.

Microhardness data:

Typical examples for microhardness values and indentations are illustrated in Figures 20, 21 and 22. The indentations were performed in areas which show mostly martensite microstructures. However, these areas are partially mixed with other constituents which obviously can lower the microhardness level and gives way to some scattering of the data. The indentations presented illustrate clearly how they are affected by the martensite before and after aging.

Obviously, there is a strong influence of the quench temperature, quench medium temperature and aging treatment on the level of microhardness. For example, the samples quenched from 940°C and 980°C exhibit measurable microhardness increase with lowering the subzero temperature. This can be attributed to the increase in the martensite content as the subzero temperature approaches the M_f temperature. On the other hand, the aging treatment of the quenched samples adds further to the hardening effect. The age hardening is clearly associated with the transformation occurring in the martensite producing adjustment of the β phase content along with the formation of secondary α . This transformation tends to create very fine particles and boundaries between phases which impede dislocation motion and thus cause hardening.

Conclusions

Subzero quench heat treatments were carried out on TC21 α/β alloy in an attempt to study the accompanying martensite transformation and developed microstructure. Quench temperatures were selected from above the β transus temperature ($T_\beta = 955^\circ\text{C}$) and below it. Post aging treatments were carried out to study their influence on the microstructure and accompanying alloy hardening. The following conclusions may be drawn:

1. Quenching from 980°C ($>T_\beta$) produces partially martensitic transformation with some retained β . Upon lowering the quench medium temperature to -20°C, the microstructure becomes largely martensitic. This finding has led to adopt -20°C as the M_f temperature for the original composition of the alloy. Additionally and following the same technique has led to adopt $M_f = -40^\circ\text{C}$ for the quenching condition from 940°C and below -40°C for quenching from 900°C.
2. Based on the data just mentioned an attempt was made to correlate the relationship between the M_f value and the parent β phase composition. This has led to an estimation of $M_f = -51^\circ\text{C}$ to the β phase composition at 900°C quench temperature and a relationship between M_f and Mo_{eq} as: $M_f (^\circ\text{C}) = -19.80 [Mo]_{eq} + 86.93$.
3. The aging treatment has led to a measurable hardness increase (over the "as-quenched" hardness) of 30-50% for 940°C depending on the subzero temperature. Also, the range of hardness increase is close to 40% for the 980°C. Considering similar data by quenching to room temperature, post aging treatment tends to raise hardness level by 8% for 940°C and by 10% for 980°C relative to before aging.
4. The formation of secondary α platelets during aging appears to be the dominating underlying hardening mechanism.
5. This prominent hardening of the subzero quenched and post aged microstructures can lead to useful overall properties of this TC21 α/β alloy.

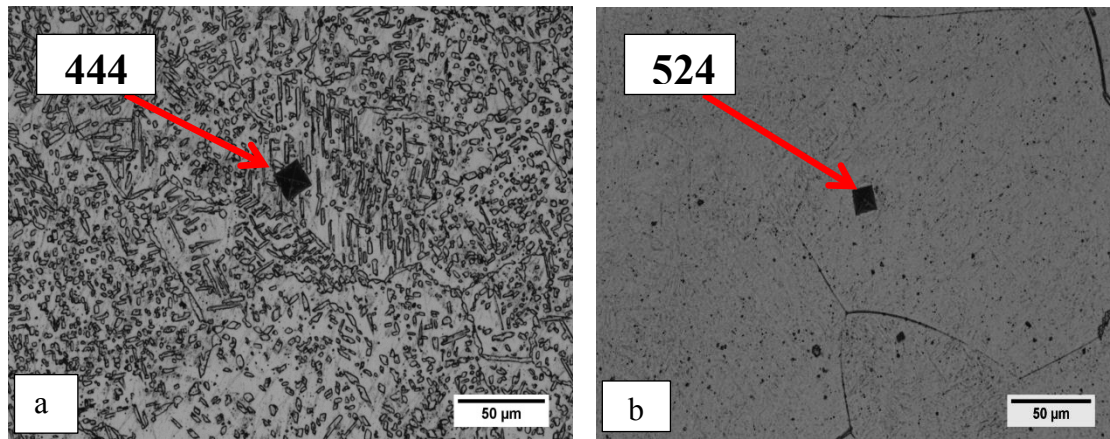


Fig. 21. Photomicrographs of microhardness indentations of: a) Sample quenched from 940 °C to -20 °C, and b) Aged condition.

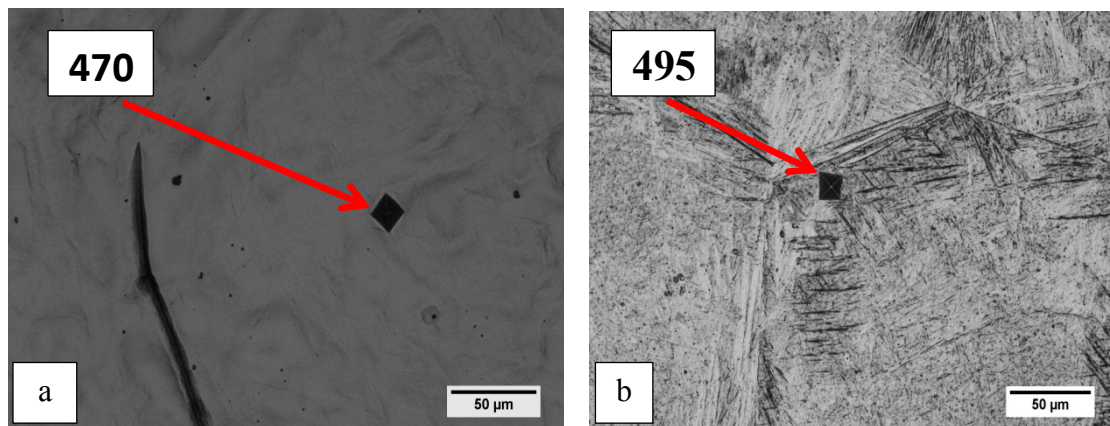


Fig. 22. Photomicrographs of microhardness indentations of: a) Sample quenched from 980 °C to 0 °C, and b) Aged condition.

Acknowledgment

* The material under investigation was gratefully supplied by CMRDI.

This paper is extracted from a PhD thesis to be submitted to the faculty of Engineering-Cairo University in partial fulfillment of the PhD degree.

References

1. Yanlei Z., Bolong L., Zhishou Z., and Zuoren N., The high temperature deformation behavior and microstructure of TC21 titanium alloy. *Mater. Sci. Eng. A*, 527, 5360-5367 (2010).
2. Zhu Y., Zeng W., Liu J., Zhao Y., Zhou Y., and Yu H., Effect of processing parameters on the hot deformation behavior of as-cast TC21 titanium alloy. *Mater. Design*, 33, 264-272 (2012).
3. Yanlei Z., Bolong L., Zhishou Z., and Zuoren N., The high temperature deformation behavior and microstructure of TC21 titanium alloy. *Mater. Sci. Eng. A*, 527, 5360-5367, (2010).
4. Changsheng T., Qiaoyan S., Lin X., Yongqing Z., and Jun S., Characterization of deformation in primary α phase and crack initiation and propagation of TC21 alloy using in-situ SEM experiments, *Mater. Sci. Eng. A*, 725, 33-42 (2018).
5. Zhi-feng S., Hong-zhen G., Jin-yang H., and Ze-kun Y., Microstructure and mechanical properties of TC21 titanium alloy after heat treatment. *Trans. Nonferrous Met. Soc. China*, 23, 2882-2889 (2013).
6. Ji-kui Z., Xiao-quan C., and Zheng-neng L., Total fatigue life prediction for Ti-alloys airframe structure based on durability and damage-tolerant design concept. *Mater. Design*, 31, 4329-4335 (2010).
7. Reham R., Adel A. N., and Abdel-Hamid A. H., Effects of quenching temperature on the mechanical properties of cast Ti-6Al-4V alloy. *J. Metall. Eng. (ME)*, 2, 48-54 (2013).
8. DĄBROWSKI R., The kinetics of phase transformations during continuous cooling of the Ti6Al4V alloy from the single-phase β range. *Arch. Metall. Mater.*, 56, 703-707 (2011).
9. Lu J., Ge P., and Zhao Y., Recent development of effect mechanism of alloying elements in titanium alloy design. *Rare Metal Eng.*, 43, 775-779 (2014).
10. Xiao-na P., Hong-zhen G., Zhi-feng S., Chun Q., and Zhang-long Z., Microstructure characterization and mechanical properties of TC4-DT titanium alloy after thermomechanical treatment. *Trans. Nonferrous Met. Soc. China*, 24, 682-689 (2014).
11. Liu W., Lin Y., Chen Y., Shi T., and Ambrish S., Effect of different heat treatments on microstructure and mechanical properties of Ti6Al4V titanium alloy. *Rare Metal Mater. Eng.*, 46, 0634-0639 (2017).
12. Ali A., Chen P., and Guo Y., Effects of microstructure on the dynamic properties of TA15 titanium alloy. *Mechanics of Mater.*, 137, 103121 (2019).
13. Ramadan N. E., Khaled M. I., Azza F. B., and Reham R. A., Fatigue Performance of Heat Treated TC21 Ti-Alloy. *Open J. Metal*, 9, 11-18 (2019).
14. Zhi-feng S., Hong-zhen G., Jian-wei Z., and Jian-ning Y., Microstructure-fracture toughness relationships and toughening mechanism of TC21 titanium alloy with lamellar microstructure. *Trans. Nonferrous Met. Soc. China*, 28, 2440-2448 (2018).
15. Xin W., Mingpan W., Chaowen H., and Min L., Strength and fracture toughness of TC21 alloy with multi-level lamellar microstructure. *Mater. Sci. Eng. A*, 740-741, 121-129 (2019).
16. Amany M. F., and Mohamed S. H., Electrochemical corrosion behavior of nano-coated Ti-6Al-4V alloy by a novel chitosan nanoparticles/silver nanoparticles in artificial saliva solution. *Egypt. J. Chem.*, 61, 747-758 (2018).
17. Hui S., Yongqing Z., Peng G., and Weidong Z., Crack initiation and mechanical properties of TC21 titanium alloy with equiaxed microstructure. *Mater. Sci. Eng. A*, 586, 215-222 (2013).
18. XU Y., LIU H., YI D., ZHU Z., and ZHENG F., Antiphase boundary-like structure in α' martensite of TC21 titanium alloy. *Trans. Nonferrous Met. Soc. China*, 22, 1366-1371 (2012).
19. Hou Z., Zhao Y., Zeng W., Mao X., Lei W., and Zhang P., Effect of heat treatment on the microstructure development of TC21 alloy. *Rare Metal Mater. Eng.*, 46, 2087-2091 (2017).

20. Bin T., Hong-Chao K., Yi-Hong W., Zhi-Shou Z., Feng-Shou Z., and Jin-Shan L., Kinetics of orthorhombic martensite decomposition in TC21 alloy under isothermal conditions. *J. Mater. Sci*, 47, 521-529 (2012).
21. LIU H., and FENG X., Microstructures and interfacial quality of diffusion bonded TC21 titanium alloy joints. *Trans. Nonferrous Met. Soc. China*, 21, 58-64 (2011).
22. Wang L. R., Ma C. L., Zhao Y. Q., and Zhou L., Effect of β heat treatment on phase transformations of TC21 during rolling. *Mater. Sci. Technol*, 32, 635-640 (2016).
23. Xin W., Mingpan W., Chaowen H., Yuanbiao T., Min L., Yilong L., and Xin C., Effect of microstructure on tensile properties, impact toughness and fracture toughness of TC21 alloy. *Mater. Design*, 180, 107898 (2019).
24. Ramadan N. M., Azza F.B., Khaled M. I., and Reham R. A., "Effect of heat treatment processes on microstructure and properties of TC21 titanium alloy". PhD thesis, Helwan University, (2017).
25. YiHong W., Hongchao K., Hui C., ZhiShou Z., XiaoFan S., Jinshan L., and Lian Z., Phase transformation in TC21 alloy during continuous heating. *J. Alloy Compd*, 472, 252-256 (2009).
26. Hui S., Yongqing Z., Peng G., and Weidong Z., Influence of Cooling Rate and Aging on the Lamellar Microstructure and Fractography of TC21 Titanium Alloy. *Metallogr. Microstruct. Anal.*, 2, 35-41 (2013).
27. Erin P. B., "Three-dimensional reconstruction of microstructures in $\alpha+\beta$ titanium alloys». Msc Thesis, Ohio State University, (2008).
28. Hiroaki M., Hiroshi Y., Kazuhisa S., Shingo K., Eric M., Damien F., Toyohiko J., and Akihiko C., Room-temperature ductility of Ti-6Al-4V alloy with α' martensite microstructure. *Mater. Sci. Eng. A*, 528, 1512-1520 (2011).
29. Yuhuan F., Lian Z., Henglei Q., Yongqing Z., and Chuazhen H., The phase and microstructure of TC21 alloy. *Mater. Sci. Eng. A*, 494, 166-172 (2008).
30. YiHong W., Hongchao K., Hui C., ZhiShou Z., FengShou Z., Jinshan L., and Lian Z., Influence of solution temperature on phase transformation of TC21 alloy. *Mater. Sci. Eng. A*, 508, 76-82 (2009).
31. Ramadan N. E., Khaled M. I., Azza F. B., and Reham R. A., Effect of duplex heat treatment on tribological behavior of TC21 titanium alloy. *J. Metall. Eng. (ME)*, 6, 1-15 (2017).
32. Pere B. V., Phase transformation kinetics during continuous heating of $\alpha+\beta$ and metastable β titanium alloys. PhD Thesis, Vienna University of Technology, (2015).
33. MASETE S., MUTOMBO K., SIYASIYA C., and STUMPF W., Effect of ageing treatment on the microstructure and hardness of the Ti6Al4V alloy. *Mater. Sci. Forum*, 828-829, 194-199 (2015).

علاقات البنية المجهرية و الصلادة في سبيكة التيتانيوم TC21 المعالجه حراريا تحت الصفر المنوى

رانيا محمد سيد الشوربجي*¹, عبدالحميد احمد حسين¹, السيد محمود البنا¹, الزهراء محمد يحيى البرادعي², محمد عبدالوهاب والي²

¹ا قسم هندسه المناجم و البترول و الفلزات, كلية الهندسة, جامعة القاهرة, الجيزة, مصر.

²مركز بحوث و تطوير الفلزات, حلوان, مصر.

تحظى سبائك التيتانيوم بقيمة كبيره من ناحية القوة و خفه الوزن و المقاومة للتآكل. و ضمن هذه السبائك تقع سبيكة TC21 (الفا + بيتا) متمتعه بهذه الخصائص بالإضافة الي مقاومتها للإنيهار. و تختص هذه السبائك بتحولها الطوري الي مارتنيسيت بالتشابه مع الصلب, مما يعطي لها قيمة عملية كوسيلة هامة لمعالجتها حراريا و التحكم في الخواص الناتجة. و في هذا الصدد فإن درجة حرارة المارتنيسيت (M_s) تعرضت للدراسة مسبقا و تحديدها اعتمادا علي التركيب الكيميائي للسبيكة. و في المقابل فإن درجة المارتنيسيت الأخرى (M_f) و اعتمادها علي التركيب الكيميائي لم تحظى بالدراسة الوافية مع أهميتها كعامل محدد للتحويل المارتنيسيتي في السبيكة. و في ضوء ذلك فقد وجهت هذه الدراسة بهدف الحصول علي تقدير كمي لهذه الدرجة و اعتمادها علي التركيب الكيميائي للسبيكة عن طريق اجراء معالجات حرارية تحت درجة الصفر المنوي. و بالإضافة لذلك تمت دراسة التصلد الناتج في السبيكة بعد اجراء هذه المعالجات الحرارية عن طريق قياسات الصلادة بشقيها الماكرو و الميكرو, و تم التوصل الي نتائج هامة في هذا الصدد مما يعطي الأمل في تحسين الخواص الميكانيكية لهذه السبائك.